The 2009 IEEE/RSJ International Conference on
Intelligent Robots and Systems
October 11-15, 2009 St. Louis, USA

Dynamical Models for Position Measurement with Global Shutter and Rolling Shutter Cameras

Edouard Laroche and Shingo Kagami

Abstract— **Vision can be used as a sensor for measuring the position of a visual marker. When the displacement of the marker over the camera exposure time is significant, the obtained position measurement is an image of the trajectory over the exposure time. This paper deals with dynamical models providing a prediction of the measurement from the continuous-time trajectory. The first contribution of the paper consists in the development of models for the global shutter and rolling shutter modes with variable exposure time. The second contribution consists in a methodology for the validation of these models. This methodology is used for validating the model of a camera with global shutter mode with full exposure time.**

I. Introduction

Vision systems with real-time image processing have been developed during the last decades and are now able to provide measurements of an object position at relatively high frequency. Based on this measurement, specific control schemes have been developed for controlling robotic manipulators [1]. Andersson developed a robot playing ping-pong based on a 60 Hz stereo vision system [2]. Nakabo et al. used a 1 000 Hz vision system in a visual loop and obtain astonishing fast results [3].

When mentioning a camera model, one generally considers the geometrical aspects, i.e. the projection model whose parameters can be estimated from a calibration procedure [4]. This model is static and concerns the formation of the image of the 3D object. When the object is moving and if its displacements over an integration period of the image are significant, the measurement provided by image processing is altered. Very few papers deal with this issue. Ranftl et al. used a simple discrete-time (DT) model of the camera for performing visual servoing for a fast ultrasonic actuator [5]. Fast dynamics can be considered as a perturbation and one then try to attenuate them [6].

The case of rolling shutter mode (RSM, also called line shutter mode) has received special attention. In this mode, the different lines are not acquired simultaneously and a variable delay appears. This phenomenon has been modelized [7] and used for estimating the 3D velocity of an object [8], [9]. These works deal with the delay from one line to another but do not deal with the displacements over the exposure time.

This latter issue is considered in this paper, i.e. the dynamical effects of vision-based position measurement. The first contribution consists in the development of models that allow to determine the DT position measurements obtained from processing one image, the input of the model being the continuous-time (CT) trajectory. Both global shutter mode (GSM) and RSM are considered; the models account for variable exposure time. The second contribution introduces a methodology for the validation of the models. It consists in projecting a moving marker with a video-projector along a predefined trajectory. This methodology is used for validating the model of a GSM camera with full-time exposition.

This work was supported by a joint funding for international collaboration from CNRS (France) and JST (Japan).

E. Laroche is with the LSIIT, Strasbourg University & CNRS, France, laroche@unistra.fr.

S. Kagami is with the Graduate School of Information Sciences, Tohoku University, Japan, swk@ic.is.tohoku.ac.jp.

II. Simplified Models

A. Measurement Method

A scene being equipped with visual markers, it is possible to measure their positions in the image by some image processing algorithm. This technique is classically used for processing visual-servoing of robots [10]. The measurements can be used directly in a 2D visual servoing scheme or can be used in order to reconstruct a 3D pose, allowing to derive 3D control. Markers are generally spots of high luminous intensity that can be detected easily. In the visible spectrum, they can be obtained by LEDs or projection of laser beams [11]. It is also possible to use a dark marker over a bright surface [12], [13]. Invisible electromagnetic radiation are also commonly used, as in the Polaris system by NDI that estimates the 3D pose from the 2D position of 3 spheres with high reflexion property in the infrared.

Usually, the elements of interest are simple circular markers and the goal of the image processing is to compute the coordinates of their centers of mass in the image. In order to limit the computation cost for real-time implementation, the image processing makes use of simple operations (binarization, threshold and computation of the center of mass).

Consider one marker and denote $(x(t), y(t))$ the coordinates of its center in the camera image. Images are acquired at the camera rate f_c. For image I_k obtained at time kT_c where $T_c = 1/f_c$, the coordinates of the marker center of mass are denoted $(\tilde{x}(k), \tilde{y}(k))$. Let neglect the noise due to the spatial discretization of the image. In a static case or if displacements are reduced over the image integration period $[(k-1)T_c, kT_c]$, one has $\tilde{x} = x$ and $\tilde{y} = y$. In the case of significant displacements over the integration period, the equality is not valid any more. In this paper, we deal with simple models allowing to compute the DT trajectory $(\tilde{x}(k), \tilde{y}(k)$ from the CT trajectory $(x(t), y(t))$. Accounting for the dynamical effects of the camera, these models are of interest for simulation, identification and control purposes.

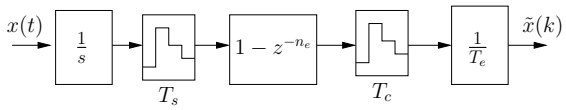

Fig. 1. Model of a camera with global shutter mode

B. Global Shutter Mode

In GSM, all the lines of image I_k are acquired over the same time interval $[kT_c - T_e, kT_c]$ where T_e is the exposure time. Assuming that the speed of the movement is constant over the exposure time and that the trajectory does not intersect itself, one can derive the following model:

$$\tilde{x}(k) = \frac{1}{T_e}\int_{kT_c-T_e}^{kT_c} x(t)\,\mathrm{d}t \quad (1)$$

$$\tilde{y}(k) = \frac{1}{T_e}\int_{kT_c-T_e}^{kT_c} y(t)\,\mathrm{d}t \quad (2)$$

Complementary details on the assumptions used for deriving this model can be found in [14]. In the case where $T_e = T_c$, this model can be easilly simulated and it is possible to account for the model of the camera when identifying a CT model of a process [14].

Hereafter, we develop a simulation model that allows $T_e \leq T_c$. Assume that T_e/T_c is rational and consider a sample time T_s and integers n_c and $n_e \leq n_c$ such that $T_c = n_c T_s$ and $T_e = n_e T_s$. For simplicity, the model is developed for coordinate x but is also valid for y. Let denote:

$$J_x(t) = \int_0^t x(\tau)\,\mathrm{d}\tau \quad (3)$$

One has:

$$\tilde{x}(k) = \frac{1}{T_e}\left(J_x(kn_cT_s) - J_x((kn_c - n_e)T_s)\right) \quad (4)$$

The model is represented in Fig. 1, including an integrator $\frac{1}{s}$, a sampler at T_s and a second sampler at T_c.

C. Rolling Shutter Mode

In RSM, lines are acquired one by one with a delay. Consider that the image is composed of n_l lines L_k numbered from 1 to n_l. Lines are acquired in increasing order, so that an image is available as soon as L_{n_l} is available. Denoting $t_k = kT_c$ the time at which image I_k is available and denoting T_d the delay between the acquisitions of the first and the last lines, line L_l is acquired over $[t_k - T_e - \frac{n-l-1}{n}T_d, t_k - \frac{n-l-1}{n}T_d]$. See Fig. 2 for the notations.

Neglecting the spatial discretization effects by considering a camera with infinite accuracy, a simplified model can be derived. Consider that y varies over $[0, \overline{y}]$. At time t, Image I_k is affected by points $(x(t), y(t))$ that satisfy the following inequalities:

$$\frac{\overline{y}}{T_d}(t_k - T_e - t) < y(t) \leq \frac{\overline{y}}{T_d}(t_k - t) \quad (5)$$

Let introduce $C_k(t)$, a binary function corresponding to Image I_k: $C_k(t) = 1$ if (5) is satisfied and $C_k(t) = 0$ otherwise. Denoting $T_r(k)$ the residence time[1] of image I_k and considering the previous assumptions, the measurement obtained from image I_k is given by:

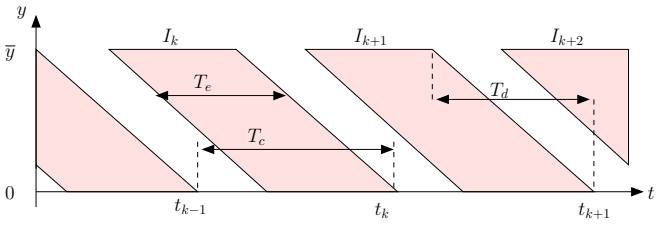

Fig. 2. Explicative time diagram for the rolling shutter mode

$$\tilde{x}(k) = \frac{1}{T_r(k)}\int_0^\infty C_k(\tau)\,x(\tau)\,\mathrm{d}\tau \quad (6)$$

$$\tilde{y}(k) = \frac{1}{T_r(k)}\int_0^\infty C_k(\tau)\,y(\tau)\,\mathrm{d}\tau \quad (7)$$

Implementing this model is not convenient as it requires the computation of many state variables. In the sequel of this subsection, a more convenient formulation relying on a limited number of state variables is given.

One very specific feature of the RSM, is that several images have to be considered at a given time t, as soon as $T_e + T_d > T_c$. The maximum number of images that are involved simultaneously writes $n_i = \mathrm{floor}(\frac{T_e+T_d}{T_c}) + 1$. The model that we propose relies on as many state variables as many images[2]. Let denote I_{xj}, $j = 0...n_i - 1$, the n_i state variables corresponding to coordinate x and I_{yj}, $j = 0...n_i - 1$, the n_i state variables corresponding to coordinate y.

For a given time t, let denote $k = \mathrm{floor}(t/T_c) + 1$ so that $t \in [t_{k-1}; t_k)$ where $t_k = kT_c$. Notice that k is time-dependent and that the reference to time is removed to lighten the notations. Depending on the value of $y(t)$, the marker contributes to image I_{k+j}, with $j = 0...n_i - 1$, if $C_{k+j}(t) = 1$. Then, we introduce the following state equations:

$$\dot{I}_{xj}(t) = C_{k+j}(t)\,x(t) \quad (8)$$

$$\dot{I}_{yj}(t) = C_{k+j}(t)\,y(t) \quad (9)$$

The measurement obtained from image I_k is finally the sum of the contributions of the different strips. For the lowest strip, the contribution over $[t_{k-1}, t_k]$ writes $I_{x0}(t_k) - I_{x0}(t_{k-1})$. The second lowest strip contributes over $[t_{k-2}, t_{k-1}]$ with $I_{x1}(t_{k-1}) - I_{x1}(t_{k-2})$ and so on if more

[1]The residence time is the length of time over which the marker contributes to a given image. In the GSM, the residence time is constant and equal to the exposure time. In the RSM, this quantity is variable, depending on the displacement of the marker. The maximum residence time is $T_e + T_d$ and can be obtained for $\dot{y} = -\overline{y}/(T_e + T_d)$ (see in Fig. 2 from point $(t_k - T_d - T_e, \overline{y})$ to $(t_k, 0)$).

[2]Notice that in practice, only one row can be readout at a time in an ordinary camera, yielding $T_d \leq T_c$ and $n_i \leq 2$. However, the model is presented in a general fashion and is also valid for $n_i > 2$.

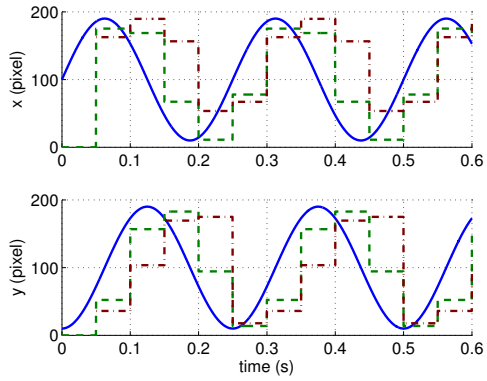

Fig. 3. Simulation results of GSM and RSM models for a circular trajectory (plain: original CT trajectory, dash: GSM, dot/dash: RSM)

strips are involved. The measurements are finally given by:

$$\tilde{x}(k) = \frac{1}{T_r(k)} \sum_{j=0}^{n_i-1} I_{xj}(t_{k-j}) - I_{xj}(t_{k-j-1}) \quad (10)$$

$$\tilde{y}(k) = \frac{1}{T_r(k)} \sum_{j=0}^{n_i-1} I_{yj}(t_{k-j}) - I_{yj}(t_{k-j-1}) \quad (11)$$

The residence time can be computed simultaneously with additional state variables. Let denote τ_0 the time length corresponding to the current image, τ_1 the time length corresponding to the next image and more generally τ_j, $j = 0...n_i$, the time length corresponding to the j^{th} future image. These states are updated according to the active mode:

$$\dot{\tau}_j(t) = C_{k+j}(t) \quad (12)$$

Finally, the residence time is computed by:

$$T_r(k) = \sum_{j=0}^{n_i-1} \tau_j(t_k) - \tau_j(t_{k-1}) \quad (13)$$

D. Simulations

For illustration, the models of the GSM and RSM were simulated with a circular trajectory at 4 Hz of center $(50, 50)$ in a 200×200 pixel image. The camera period is T_c = 50 ms and the exposure time is 20 ms. The GSM is implemented with T_s = 10 ms, $n_e = 2$ and $n_c = 5$. For the RSM, a delay $T_d = T_c$ = 50 ms is considered. The original CT trajectory and the DT trajectories obtained with the two modes are given in Fig. 3. One can notice that the measurement obtained with GSM has a constant delay whereas the measurement obtained with RSM has a variable delay that increases with y position. This behavior is in accordance with the analysis presented earlier in this section.

III. Experimental Validation

This section presents an experimental validation of the model of the GSM with full exposure time.

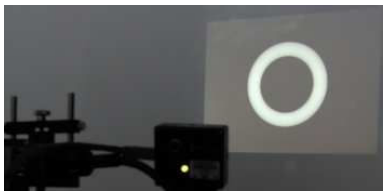

Fig. 4. View of the setup; on the frontground: the camera (right) and the videoprojector (left); on the background: the screen

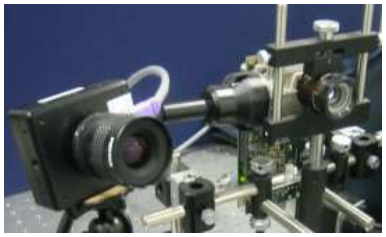

Fig. 5. Partial view on the camera (left) and the videoprojector (right)

A. Evaluation method

For experimental validation of our models, it is required to move a marker at high speed along a given trajectory in a reliable and reproducible way. For this purpose, we use a high-speed video projector [15] that projects a spot on a screen. A periodic trajectory is chosen and images are acquired by the camera of frequency $f_c = 1/T_c$. Assuming that the projector rate f_p is high, the displacement of the spot can be considered as continuous and the obtained images are equivalent to those obtained by the displacement of a LED on a moving arm. Assuming that the corresponding CT trajectory in the camera frame is know, the model (1-2) will be used for predicting the measurements. These predictions will be compared with the measurements based on image processing, allowing to evaluate the model. Comparisons will be done with other models available in the literature.

The steps required for validating the model are: (i) choose a trajectory in the projector frame; (ii) identify the corresponding trajectory in the camera frame; (iii) acquire the images for the corresponding trajectory; (iv) compute the prediction based on the model; (v) synchronize the data (in the case where no synchronization between camera and projector is available); (vi) compare the output data. In the results presented herein, a circular trajectory was chosen.

B. Description of the Setup

The experimental system, as shown in Fig. 4 and 5, consists of a high-speed projector that generates marker patterns and a CCD camera that captures images of the marker. The projector and the camera are set approximately side by side at the distance of about 200 mm from each other. A planar screen is set at the distance of about 700 mm in front of the projector-camera system. The optical axes of the projector and the camera are not parallel to each other, which makes the captured marker trajectory an incomplete circle.

The projector is composed of a Texas Instruments Digital Micromirror Device [16] DMD 0.7XGA 12 DDR, its con-

troller board DMD Discovery 1100 and an external memory board ViALUX ALP-1. In this configuration, $1\,024 \times 768$ pixels binary images can be projected at up to 8 kHz. In the presented experiments, The maximum projection frame rate is set at $f_{p_{\max}} = 4$ kHz to ensure stable operations. The external memory board is able to store up to $n_{\max} = 2\,730$ frames, and an arbitrary binary image sequence whose length is within $n_{\max}$ frames can be projected repeatedly. Light from a metal halide lamp Fiber-Lite MH-100 is guided to the DMD by an optical fiber guide, and the light reflected by the DMD is projected through a lens whose focal length is about 27 mm. Since a single mirror size of the DMD is 13.68 μm, the horizontal view angle is about 29 degree.

The camera is a Point Grey Research Dragonfly Express IEEE1394b camera, which captures 640×480-pixel 8-bit monochrome images with the progressive scan in GSM. In the presented experiments, images are acquired at $f_c = 50$ Hz with full-time exposure ($T_e = T_c$). The focal length of the camera lens is about 6 mm and the CCD pixel size is 7.4 μm, resulting in the horizontal view angle of about 43 degree.

For illustration, an image obtained with this system is given in Fig. 6.a, in addition with the measurements of the center of mass obtained with and without Sobel filter. The corresponding binary images are given in Fig. 6.b and 6.c.

C. Trajectory Design

Consider a given periodic trajectory of frequency $f = 1/T$. It is necessary to choose the corresponding number of projector patterns n and projector rate f_p that satisfy the contraints $n \leq n_{\max}$ and $f_p < f_{p\max}$. Let denote T_g the period of the aquisition. It is convenient that T_g is composed of multiple periods of both the trajectory, the camera and the projector. This is the case as soon as the exist intergers n, k_1 and k_2 such that:

$$T_g = nT_p = k_1 T = k_2 T_c \tag{14}$$

where $T_p = 1/f_p$. In order to maximize the accuracy, the projector rate f_p is maximized.

Each projected image is composed of a white point of radius r at a particular position on a circle of center (x_0, y_0) and radius R. The trajectory in the projector frame writes $x_p(t) = x_0 + R\cos(\phi(t))$, $y_p(t) = x_0 + R\sin(\phi(t))$ where the phase $\phi(t)$ can be chosen arbitrarily. The center of the trajectory is chosen as the center of the image. The trajectory radius is chosen as $R = 200$ pixels. For most of the tests, we chose $r = 40$ pixels. However, experiments with different values of r are processed. The global period being T_g, $n = T_g f_p$ frames are computed at the projector frequency, based on $\phi_k = \phi(kT_p)$, $k = 0 \cdots n-1$.

D. Identification of the Trajectory in the Camera Frame

As the trajectory $(x_p(\phi), y_p(\phi))$ in the projector frame, the trajectory in the image frame $(x(\phi), y(\phi))$ is periodic of periodicity 2π. Whereas the trajectory in the projector frame is well-known, as it is chosen by the user, the knowledge of the trajectory in the image frame requires some attention. Developing a projective model would require the estimation of many parameters and estimation errors would introduce reconstruction errors. A more simple approach can be used, taking profit of the periodicity of the trajectories, consisting in identifying a truncated Fourier series of respectively $x(\phi)$ and $y(\phi)$:

$$x(t) = a_0 + \sum_{k=1}^{m} a_k \cos(k\phi) + b_k \sin(k\phi) \tag{15}$$

$$y(t) = c_0 + \sum_{k=1}^{m} c_k \cos(k\phi) + d_k \sin(k\phi) \tag{16}$$

Parameters are evaluated by linear regression in order to fit static measurements. A number of 1024 positions regularly spaced was chosen. Order $m = 2$ was chosen for the truncation, allowing an accuracy around 0.13 pixel, which is close to the residual measurement error.

λ	k_1	k_2	k_1/k_2	T_g (ms)	n
0.1	1	10	0.1	200	800
0.192	1	8	0.125	160	640
0.167	1	6	0.167	120	480
0.215	1	5	0.2	100	400
0.278	3	11	0.272	220	880
0.359	1	3	0.333	60	240
0.464	6	13	0.462	260	1040
0.599	3	5	0.6	100	400
0.774	3	4	0.75	80	320
1	1	1	1	20	80

TABLE I

NUMERICAL VALUES OF THE PARAMETERS OF THE CONSTANT VELOCITY EXPERIMENT; T_g IS THE GLOBAL PERIOD AND n IS THE NUMBER OF FRAMES.

E. Evaluation Results

1) Constant velocity trajectories: The phase of the trajectory writes $\phi(t) = 2\pi f t$. Different experiments were processed with f varying from $f_c/10$ up to f_c. Let denote $\lambda = f/f_c$ this frequency ratio that should vary from 0.1 to 1. Making use of the explanations of Section III-B, k_1 and k_2 were chosen such that k_1/k_2 is close to the desired value of λ. The maximum projector rate $f_p = 4$ kHz was used for each case. The parameters obtained for the different λ are given in Table I.

As a sample, the results for $\lambda = 0.359$ are given in Fig. 7. One can notice that the model allows a very accurate prediction of the measurements. For evaluation and comparison, the RMS errors obtained for the different values of f/f_c are given in Fig. 8 considering 5 different models (M1 to M5):

- M1. Model for GSM and full exposure time presented in the paper
- M2. Mean of the values at the beginning and at the end of the interval ($\tilde{x}(k) = \frac{1}{2}(x((k-1)T_c) + x(kT_c))$) [5]
- M3. Position at the beginning of the interval ($\tilde{x}(k) = x((k-1)T_c)$)
- M4. Position at the end of the interval ($\tilde{x}(k) = x(kT_c)$)
- M5. Position at the middle of the camera interval ($\tilde{x}(k) = x((k-\frac{1}{2})T_c)$)

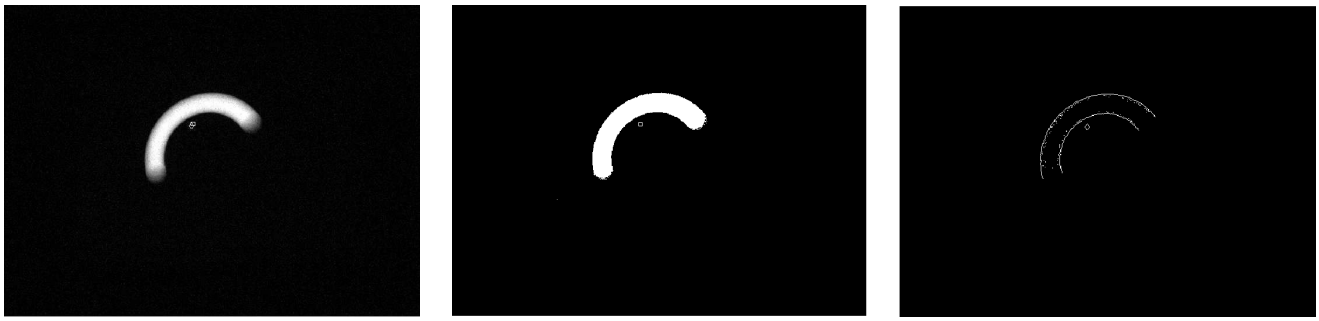

a. *b.* *c.*

Fig. 6. Images obtained by the camera and image processing in addition with the position measurements. a/ original image and the measurements (□: without Sobel filter; ◇: with Sobel filter); b/ binary image obtained without Sobel filter and its center of mass (□); c/ binary image obtained with Sobel filter and its center of mass (◇)

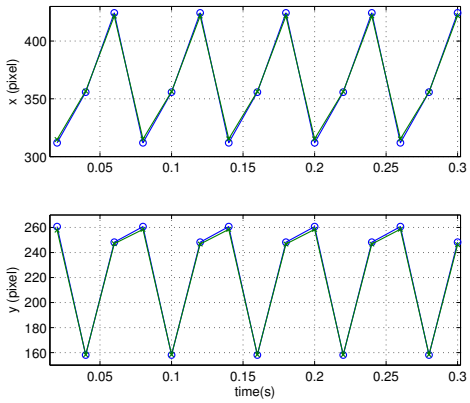

Fig. 7. Measurements (×) and predicted values (○) for $\lambda = 0.359$

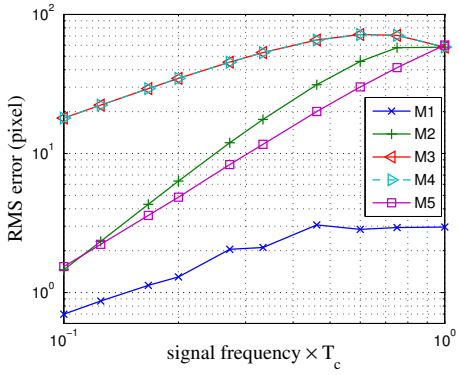

Fig. 8. Variations of the prediction errors obtained with the different models with respect to f/f_c

One can notice that the model developed in this paper is by far the more accurate. This is notably the case when the signal frequency is close to the camera rate. Whereas the RMS errors remains lower than 3 pixels with the proposed model, it reaches several dozens with the other models. One can also notice that models M2 and M5 are efficient for the low frequencies, but the prediction errors increase for frequencies close to the camera rate.

2) Trajectories with varying velocity: Model M1 relies on the assumption that the trajectory has constant velocity amplitude. Therefore, it is worth evaluating how the accuracy of the model degrade when this assumption is not satisfied any more. For this purpose, a trajectory with varying velocity was implemented: $\mathrm{d}\phi/\mathrm{d}t = \omega(t)$ where ω is varying linearly up and down from $\omega_{\min}$ to $\omega_{\max}$ with periodicity T_ω.

Let compute a trajectory such that after a given number k_2 of periods T_ω, the position of the marker comes back to the initial position. The phase shift after one period T_ω is $\Delta_\theta = T_\omega(\omega_{\max} + \omega_{\min})/2$. Imposing $\Delta_\theta = 2\pi\, k_1/k_2$, with $k_1, k_2 \in \mathbb{N}^+$, then the target will make k_1 turns in k_2 periods T_ω.

In addition, let insure that the periodicity of the displacement is commensurable with the camera period so that the measurement provided by the camera will be periodic, i.e. find $k_3, k_4 \in \mathbb{N}^+$ such that $T_\omega = T_c k_3/k_4$. The common periodicity of T_c and T_ω is $k_4 T_\omega = k_3 T_c$. Then the global periodicity of the system writes $T_g = k_5 T_\omega$ where k_5 is the least common multiplier of k_2 and k_4.

The following results were obtained with $k_1 = 3$, $k_2 = 2$, $k_3 = 7$ and $k_4 = 3$. We obtain $T_\omega = 46.7$ ms. The global period is $T_g = 6\,T_\omega = 14\,T_c = 280$ ms, corresponding to 1120 frames at 4 kHz. By choosing $w_{\max} = 2\pi f_c = 314$ rad/s, it results in $w_{\min} = 89.8$ rad/s.

This trajectory was implemented on the setup and the computation of the center of mass was made with different threshold. The RMS errors for different thresholds and the different methods are given in Table II. One can notice that Model M1 is not as good as in a constant velocity situation (16 pixel error instead of 3); nevertheless, the results remains far more accurate than with the other models (the error remains almost three times lower).

3) Varying the spot radius and the detection algorithm: The model assumes that the radius of the spot is small compared to the radius of the trajectory. The models were evaluated with markers of different radii r. The results obtained with a trajectory at constant speed module with $k_1 = 3$ and $k_3 = 5$ are given with two processing protocols:

- with threshold and center of mass, Fig. 9,
- with Sobel filter, threshold and center of mass, Fig. 10.

σ	M1	M2	M3	M4	M5
0.1	16	49	70	68	62
0.2	16	51	72	69	62
0.3	16	52	72	69	63
0.4	17	53	73	69	64
0.5	20	53	74	69	67

TABLE II

TESTS WITH VARIABLE SPEED: RMS (IN PIXEL) OF THE ESTIMATION ERROR FOR DIFFERENT THRESHOLD σ AND THE DIFFERENT MODELS

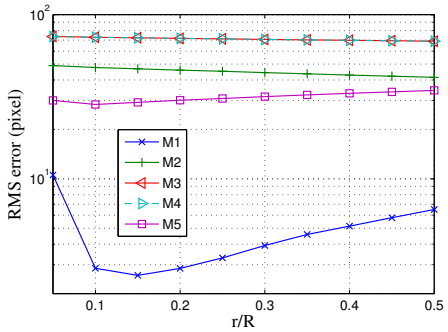

Fig. 9. Influence of the marker radius without Sobel filter

One can notice that the estimation error varies with respect to r/R. Let focus on Model M1. As expected, the error globally increases with r/R. In the case witout Sobel filter, the RMS error is higher for the very low r/R ($r/R \leq 0.15$). Indeed, in this situation, images receive few light and the detection of the center of mass is hazardous. Assuming that the marker is sufficiently luminous, model M1 is more accurate without using the Sobel filter.

IV. CONCLUSION

The dynamical models developed in this paper allow to predict the position measurement given by a camera in the case of significant displacements over the integration period. These models are useful in situations where a CT model of a process or robot is to be obtained from the DT measurements given by camera. Devices including fast dynamics or vibrations are particularly concerned. New models were introduced in this paper that allow to account for the dynamical effects of the GSM and RSM cameras with various exposition time. All these models can be implemented and used in simulation.

In addition, an evaluation procedure was detailed in the paper. Applied to a model with GSM and full exposure time, this evaluation showed that the proposed model provides a very accurate estimation of the measurement in situations where the modulus of the velocity remains constant over the integration period. Thanks to this evaluation procedure, we were able to quantify the variations of the measurement errors with respect to size of the marker. These variations remains low, even with fast displacements of the marker. We were also able to quantify the effects of the image processing algorithm on the measurement accuracy. It results that the model is generally more accurate without the use of a Sobel filter, except in low exposition situation.

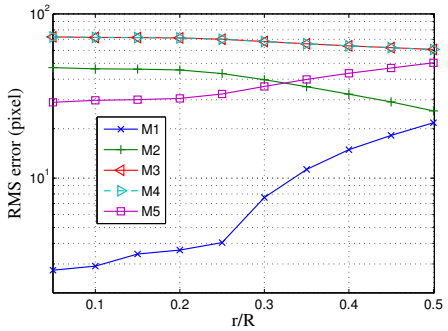

Fig. 10. Influence of the marker radius with Sobel filter

REFERENCES

[1] P. Corke, *Visual control of robots*. Taunton, Somerset, U.K.: Research Studies Press Ltd., 1996.

[2] R. Andersson, "Dynamic sensing in a ping-pong playing robot," *IEEE Trans. Robot. Autom.*, vol. 5, no. 6, pp. 728 – 739, 1989.

[3] Y. Nakabo, M. Ishikawa, H. Toyoda, and S. Mizuno, "1 ms column parallel vision system and its application of high speed target tracking," in *Int. Conf. Robot. Autom.*, vol. 1, 2000, pp. 650 – 655.

[4] M. Brown, A. Majumder, and R. Yang, "Camera-based calibration techniques for seamless multiprojector displays," *IEEE Trans. Visual. Comput. Graphics*, vol. 11, no. 2, pp. 193 – 206, 2005.

[5] A. Ranftl, L. Cuvillon, J. Gangloff, and J. van der Sloten, "High speed visual servoing with ultrasonic motors," in *Int. Conf. Robot. Autom. (ICRA)*, April 2007.

[6] C. Luna, M. Mazo, J. Lazaro, J. Vazquez, J. Urena, S. Palazuelos, J. Garcia, F. Espinoza, and E. Santiso, "Method to measure the rotation angles in vibrating systems," *IEEE Trans. Instrum. Measurement*, vol. 55, no. 1, pp. 232–239, 2006.

[7] M. Meingast, C. Geyer, and S. Sastry, "Geometric models of rolling-shutter cameras," in *Workshop on Omnidirectional Vision, Camera Networks and Non-Classical Cameras*, Beijing, China, 2005.

[8] O. Ait-Aider, N. Andreff, J. Lavest, and P. Martinet, "Exploiting rolling shutter distortions for simultaneous object pose and velocity computation using a single view," in *IEEE International Conference on Computer Vision Systems*, New York, USA, 2006.

[9] O. Ait-Aider, A. Bartoli, and N. Andreff, "Kinematics from lines in a single rolling shutter image," in *IEEE International Conference on Computer Vision and Pattern Recognition*, Minneapolis, Minnesota, USA, 2007.

[10] S. Hutchinson, G. D. Hager, and P. I. Corke, "A tutorial on visual servo control," *IEEE Trans. Robot. Autom.*, vol. 12, no. 5, pp. 651–670, 1996.

[11] A. Krupa, J. Gangloff, C. Doignon, M. de Mathelin, G. Morel, J. Leroy, and L. Soler, "Autonomous 3-D positioning of surgical instruments in robotized laparoscopic surgery using visual servoing," *IEEE Trans. Robot. Autom.*, vol. 19, no. 5, pp. 842 – 853, 2003.

[12] J. Gangloff and M. de Mathelin, "High speed visual servoing of a 6 DOF manipulator using multivariable predictive control," *Advanced Robotics*, vol. 17, no. 10, pp. 993–1021, 2003.

[13] W. Bachta, P. Renaud, E. Laroche, J. Gangloff, and A. Forgione, "Progress towards a robotized heart stabilizer design and control," in *Int. Conf. Intelligent Robots and Systems*, San Diego, Ca, USA, 2007.

[14] E. Laroche and J. Delavigne, "Dynamical effects of vision-based position measurement," in *IFAC World Congress*, Seoul, South Korea, 2008.

[15] J. Takei, S. Kagami, and K. Hashimoto, "3,000-fps 3-D shape measurement using a high-speed camera-projector system," in *2007 IEEE/RSJ International Conference on Intelligent Robots and Systems*, 2007, pp. 3211–3216.

[16] D. Dudley, W. Duncan, and J. Slaughter, "Emerging digital micromirror device (DMD) applications," *Proceedings of SPIE*, vol. 4985, 2003.